scientific reports

OPEN

A coiled-coil-based design strategy for the thermostabilization of G-protein-coupled receptors

Marwa Amer, Oneda Leka, Piotr Jasko, Daniel Frey, Xiaodan Li & Richard A. Kammerer[✉]

Structure elucidation of inactive-state GPCRs still mostly relies on X-ray crystallography. The major goal of our work was to create a new GPCR tool that would provide receptor stability and additional soluble surface for crystallization. Towards this aim, we selected the two-stranded antiparallel coiled coil as a domain fold that satisfies both criteria. A selection of antiparallel coiled coils was used for structure-guided substitution of intracellular loop 3 of the β3 adrenergic receptor. Unexpectedly, only the two GPCR variants containing thermostable coiled coils were expressed. We showed that one GPCR chimera is stable upon purification in detergent, retains ligand-binding properties, and can be crystallized. However, the quality of the crystals was not suitable for structure determination. By using two other examples, 5HTR2C and α2BAR, we demonstrate that our approach is generally suitable for the stabilization of GPCRs. To provide additional surface for promoting crystal contacts, we replaced in a structure-based approach the loop connecting the antiparallel coiled coil by T4L. We found that the engineered GPCR is even more stable than the coiled-coil variant. Negative-staining TEM revealed a homogeneous distribution of particles, indicating that coiled-coil-T4L receptor variants might also be promising candidate proteins for structure elucidation by cryo-EM. Our approach should be of interest for applications that benefit from stable GPCRs.

G-protein-coupled receptors (GPCRs) are characterized by a seven-transmembrane helix topology and represent the largest membrane protein family[1]. GPCRs play fundamental roles in almost all physiological and pathological processes by responding to a variety of extracellular signals, including photons, small molecules, peptides and proteins. These signals cause conformational changes in the GPCR and lead to the activation of associated G proteins that regulate central downstream signaling pathways[2,3]. GPCRs are the target of approximately 30% of all approved drugs on the market and are therefore of enormous medical and commercial interest[4–6]. Despite AlphaFold2[7] and RoseTTAfold[8] that both can predict apo-structures to a high degree of accuracy, there is a growing demand on high-resolution structures of GPCR/ligand complexes for structure-based drug design. Cryo-electron microscopy (cryo-EM) represents nowadays the method of choice for determining active-state GPCR structures in complex with heteromeric G proteins[9], but the method is limited for structure elucidation of inactive-state receptors, in particular family A GPCRs, as a result of size. This limitation severely affects structure-based drug discovery because about half of the drugs target inactive-state receptors. Although a universal nanobody holds huge promise for the structure determination of inactive-state receptors[10], structure elucidation of inactive-state GPCRs currently still mostly relies on X-ray crystallography. However, generating GPCRs suitable for X-ray structural studies is a challenging subject because of their poor expression, conformational heterogeneity, and stability that affects purification and crystallization[11]. Accordingly, the determination of available GPCR crystal structures was the result of extensive modifications that often required a combination of several of the following protein engineering approaches: (1) truncation of unstructured N- and/or C-termini and/or loops, (2) scanning alanine mutagenesis (SAM), (3) application of fusion proteins, such as bacteriophage T4 lysozyme (T4L), thermostabilized cytochrome b562RIL (BRIL), flavodoxin, xylanase, rubredoxin, neuraminidase A glycogen synthase, or arrestin, (4) removal of post-translation modification sites, (5) stabilization by antibodies, nanobodies and DARPins and thermostabilization by computational design[10–17].

The most common methods used for crystallizing GPCRs are SAM[18] and the fusion protein approach[19,20]. The rationale behind SAM is to create stable and conformation-specific GPCRs while maintaining their pharmacological activity. Systematically, single amino acid mutants of a GPCR of interest are generated by substituting each amino acid in the sequence with Ala (Gly if the wild-type residue is an Ala). Typically, the most stabilizing mutations are then combined until a mutant with the desired stability is obtained. This method was for example

Laboratory of Biomolecular Research, Division of Biology and Chemistry, Paul Scherrer Institute, 5232 Villigen PSI, Switzerland. ✉email: richard.kammerer@psi.ch

successfully employed for solving the structure of the β1 adrenergic receptor[21] and the C–C chemokine receptor type 9[22]. A major disadvantage of SAM is that the method is rather labor-intensive. Moreover, the stabilized GPCR might still require further protein engineering to generate the necessary soluble surface area needed for crystallization in detergent[23].

Extension of the relatively small polar surface area of GPCRs that is available for forming crystal lattice contacts is the rationale behind the fusion protein engineering approach[19,20]. Typically, partner proteins such as T4L, bRIL and others are fused to the truncated N-terminus of a GPCR or replace the unstructured intracellular loop 3 (ICL3)[11]. Using this approach, the crystal structures of more than 40 receptors were determined, including those of the β2 adrenergic receptor[19,20], the chemokine CXCR4 receptor[24], the OX2 orexin receptor[13] and the CC chemokine receptor 7[12]. Not all GPCRs are amenable to fusion protein engineering, and it appears that the approach is suitable for GPCRs only that when bound to a stabilizing ligand are stable upon detergent solubilization from their membrane environment.

Based on the available crystal structures, it seems that a combination of both SAM and the fusion protein approach would be the most promising strategy for the efficient crystallization of GPCRs. The major goal of our work was to create a new GPCR tool that would provide receptor stability and additional crystallizable surface at the same time. Toward our aim, we selected the α-helical coiled coil as a candidate because coiled coils are generally very soluble and can fold into very stable structures. Furthermore, short coiled coils typically can be easily crystallized and resulting crystal structures are frequently determined at high resolution. The left-handed coiled coil is probably the most widespread subunit oligomerization motif found in proteins[25]. It consists of two or more amphipathic α-helices that "coil" around each other in a left-handed supertwist. It is characterized by a heptad-repeat sequence of seven amino-acid residues denoted $[abcdefg]_n$ (Fig. 1) with a 3,4-hydrophobic repeat of mostly non-polar amino acids at positions a and d. Interactions between the a and d core residues and its flanking e and g positions determine the stability of a coiled coil, the number of strands it consists of, the parallel or antiparallel orientation of α-helices, and the homo- or heterotypic association of subunits. We and others previously used coiled coils to successfully stabilize proteins/peptides[26–29].

A selection of different two-stranded antiparallel coiled-coil structures, in which the same polypeptide chain folds back on itself, were used to replace ICL3 of the β3 adrenergic receptor (β3AR). Expression, solubilization in detergent, analytical size exclusion chromatography, binding studies, X-ray crystallography and EM were performed, to assess the effect of the coiled coils on the functionality, stability and feasibility for structural work
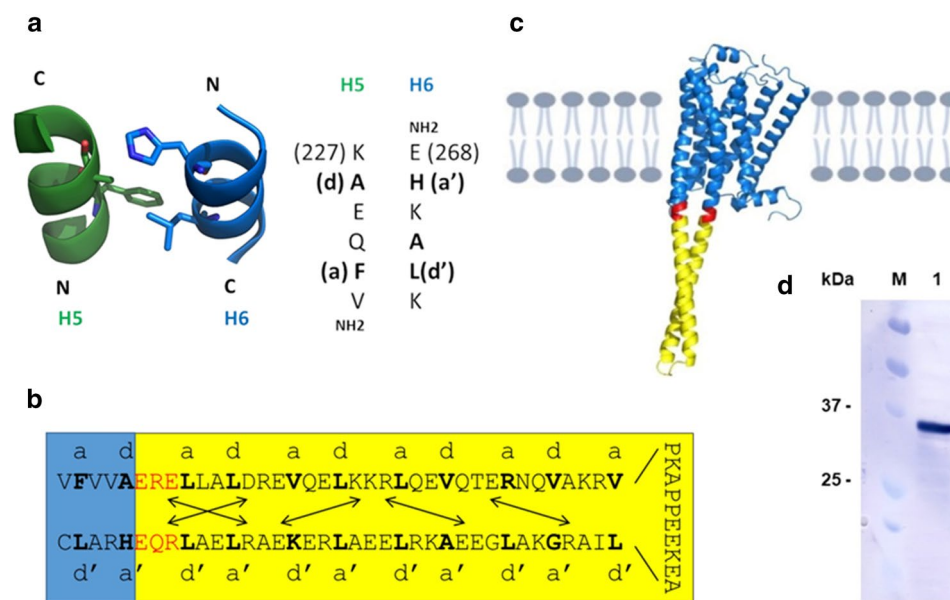
Figure 1. Design rationale of β3AR-coiled-coil chimeras. (**a**) Side view (left panel) of ribbon representation of crystal structure of β2-adrenergic receptor transmembrane helices 5 (green) and 6 (blue) that interact in an antiparallel coiled-coil like manner at the cytosolic side (PDB code: 2RH1)[19]. Interacting amino-acid residues are shown as sticks. Sequences of the interacting segments of transmembrane helices 5 and 6 are shown in the right panel. Residues at the hydrophobic heptad-repeat positions a, a′, d and d′ are shown in bold and numbered according to their position in the wild-type protein. N- and C-termini are indicated. (**b**) Example of chimeric β3AR. In-register heptad-repeat fusion of the antiparallel coiled coil of the *Thermus thermophilus* seryl-tRNA synthetase (SRS, cc3.1) (yellow) and the human β3-adrenergic receptor (blue). Introduction of three amino-acid residues at the junction (red) was necessary to obtain a continuous heptad-repeat pattern. Amino-acid residues at the e′ and f positions of the junction were chosen to introduce two additional attractive salt bridges into cc3.1 and potentially further stabilize the protein. The heptad-repeat pattern is indicated. Potential salt bridges are indicated by arrows. (**c**) β3AR-cc3.1 model. β3AR is shown in blue, the cc3.1 coiled coil in yellow and residues at the junction in red. The model was generated by AlphaFold2[7]. (**d**) Western blot analysis demonstrating the expression of B3AR-cc3.1 (lane 1). The migration of marker proteins is shown (M).

of the chimeric receptor. Using two additional receptors, the 5-hydroxytryptamine receptor 2C (5HTR2C) and the α-2B adrenergic receptor (α2BAR), we tested the general suitability of our approach.

Results and discussion

Design rationale of engineered GPCR variants.

The design rationale of our GPCR variants is based on the observation that at the cytoplasmic site in the crystal structure of β2AR, transmembrane helices 5 and 6 are interacting over a short stretch of residues in a way that is very similar to an antiparallel coiled coil[19] (PDB code: 2RH1). Specifically, residues Phe223 and Ala226 of helix 5 that can be assigned the hydrophobic heptad-repeat positions *a* and *d*, respectively, interact with His269 and Leu272 at positions *a′* and *d′*, respectively, of helix 6 (Fig. 1a). β3AR was selected because it is the closest relative of β2AR, for which no high-resolution structure was available at the time. The idea behind the design was to replace ICL3 of β3AR by a series of antiparallel coiled coils and thereby extend the sequence corresponding to coiled-coil-like structure seen in β2AR (Fig. 1b,c). The coiled coil would therefore act like a clamp on β3AR transmembrane helices 5 and 6 that would hopefully stabilize the entire GPCR and provide additional soluble surface for crystallization. The coiled coils were inserted into ICL3 between Ala231 and Glu286 (Fig. 1b). Coiled-coil positions *e, e′, g* and *g′* that flank the hydrophobic *a, a′, d* and *d′* positions are frequently occupied by charged residues that form *g* to *g′* and *e* to *e′* type salt bridges that can further stabilize the structure[30]. To this end, amino-acid residues at the junction were chosen to optimize attractive electrostatic interactions between helices (Fig. 1b).

Towards this end, the RCSB Protein Data Bank, CC+[31] and the literature was screened to identify suitable antiparallel coiled-coil candidates for substituting ICL3 of β3AR. The main criterion for selecting coiled coil fusion partners was that they form a stable two-stranded antiparallel structure alone. This applied to all the coiled coils except cc6, which, based on its extended structure, is likely to be stable alone. Ideally, a crystal structure would be available for the candidate coiled coils. Furthermore, we were also searching for coiled coils with different properties, including size, stability, self-interaction or additional structures. The heptad-repeat register was identified from the papers and the PDB files describing the structures and compared to coiled-coil prediction algorithms and analysis software.

Based on their characteristics, six antiparallel coiled coils were selected (Supplementary Fig. S1 and Supplementary Table S1). cc1 is derived from a bacteriophage serine integrase that plays a key role in the integration of the viral genome through self-interactions between the coiled-coil domains[32]. Based on its small size (three heptad repeats), the coiled coil is not expected to affect G-protein binding of the β3AR chimera. cc2 originates from a viral nucleocapsid protein[33] and like cc1 can interact with itself. The capability to self-interact makes cc1 and cc2 promising candidates to establish potential crystal contacts between chimeric β3AR-cc molecules. Coiled coils from thermostable proteins are potentially extremely stable and attractive candidates to stabilize β3AR. Towards this aim, the antiparallel coiled-coil domains of seryl-tRNA synthetase (SRS) from *Thermus thermophilus* (cc3.1)[34] and *Pyrolobus fumarii* (cc3.2), bacteria that can grow in extreme temperature conditions of up to 85 °C and 122 °C, respectively, were selected. Although high-resolution structures of the isolated thermostable coiled-coils are not available for the proteins, the domain from *E. coli* has been characterized in detail[35]. Coiled-coil candidates with defined additional α-helical structures instead of the loop connecting the two helices were also selected because they provide a larger surface for crystallization than classical antiparallel coiled coils. cc4 is derived from the pore-forming toxin YaxAB[36] and cc5 represents the microtubule-binding domain from dynein[37].

Covalent connection of helices by disulfide bonds at their N- or C-terminus is a common approach to stabilize coiled-coil structures[35,38]. Because some of the isolated coiled-coil candidates are potentially not very stable, a second series of β3AR chimeras harboring an intramolecular disulfide bond, termed βAR3-cc_SS, was designed to increase their stability (Supplementary Fig. S1 and Supplementary Table S1).

Based on the secondary structure prediction, truncation of the predicted unstructured N- and C-terminus of human β3AR was carried out. Specifically, 25 N-terminal residues (Pro3 to Thr27) that contain two potential N-glycosylation sites (amino-acid residues Asn8 and Asn26) and the C-terminal 40 residues after the palmitoylation site (Pro369 to Ser408) were deleted.

Residue substitutions were identified that thermostabilized the turkey β1AR[18,39]. The combination mutant was significantly more stable than the native protein when solubilized in dodecylmaltoside (DDM) and in short chain detergents, which allowed its crystallization and structure determination. Because it was shown that the mutations could be transferred from β1AR to β2AR[40], the β3AR sequence was further modified by introducing the following mutations: Glu36Ala, Met86Val, Ile125Val, Glu126Trp, Tyr234Ala, Phe341Met, and Tyr346Leu[39].

We selected this structure-based "all-in-one" approach because we never obtained expression of wild-type β3AR. Therefore, we didn't consider truncation of the wild-type a promising approach to obtain expression levels required for structural work. With our in-register coiled-coil fusion approach, we furthermore intend to demonstrate that the testing of multiple fusion sites or multiple constructs at the same fusion site are actually not required.

Only β3AR-cc chimeras fused to thermostable coiled coils exhibit expression.

Three different cell lines, HEK293S GnTI⁻, T-REx-293, T-REx-CHO, were screened for the expression of the 12 β3AR chimeras. Only β3AR-cc3.1 (Fig. 1d) and β3AR-cc3.2 showed reasonable expression levels in T-REx-293 cells. The expression level of β3AR-cc3.1 was higher compared to the one of β3AR-cc3.2. Instead, the other tested variants did not express in any of the cell lines. These results suggest that the stability of GPCRs is an important factor for expression, a hypothesis that is consistent with that we were unable to express wild-type β3AR as a control. They furthermore demonstrate that thermostable coiled coils are promising fusion candidates for GPCR stabilization and that the stabilizing mutations identified for β1AR had no stabilizing effect on β3AR.

The observation that the disulfide-linked variants of the β3AR-cc3.1 and β3AR-cc3.2 chimeras did not express can be rationally explained by destabilization of the coiled coils upon introducing Cys residues. Hydrophobic amino acids like Leu, Ile or Val at heptad repeat *a* and *d* positions are mainly responsible for the stability of a coiled coil and substitution of such a residue usually leads to a significant destabilization of the structure[41,42].

As a result of its higher expression, we focused on β3AR-cc3.1 and generated stable cell lines expressing chimeric protein. Notably, addition of both tetracycline (2 μg/mL) and sodium butyrate (5 mM) resulted in a three-fold increase in the expression efficiency.

β3AR-cc3.1 is stable upon solubilization and purification in detergent.

To identify the best detergent for solubilization, a screen of representative detergents from different families covering a wide range of chemical properties was carried out. To this aim, (*n*-dodecyl-β-ᴅ-maltopyranoside (DDM) (maltoside detergent group), lauryl maltose neopentyl glycol (LMNG) (NG class detergent group), undecanoyl-*n*-hydroxyethylglucamide (HEGA11) (HEGA detergent group), *n*-decyl-β-ᴅ-thiomaltoside (DDTM) (thio maltoside detergent group), *n*-dodecylphosphocholine (FC12) (lipid-like detergent group), 5-cyclohexyl-1-pentyl-β-ᴅ-maltoside (CYMAL7) (CYMAL detergent group) and *n*-dodecyl-β-ᴅ-glucopyranoside (DDG) (glucoside detergent group) and *n*-decyl-β-ᴅ-glucopyranoside (DTG) (thio glucoside detergent group) were tested. Each detergent was assessed for its ability to solubilize β3AR-cc3.1 at a final concentration of 1% (w/v), a concentration that is at least 100 times above the CMC values of the tested detergents. Western blot analysis using an anti-FLAG monoclonal antibody demonstrated that all the detergents efficiently solubilized β3AR-cc3.1 (Fig. 2a).

Next, a small-scale purification of β3AR-cc3.1 using StrepTrap Sepharose beads was performed for each detergent as described in the Materials and Methods section. SDS-PAGE analysis demonstrated that β3AR-cc3.1 could be efficiently purified with all the tested detergents. For most detergents, a single band of β3AR-cc3.1 migrating at approximately 42 kDa was detected, but for LMNG, DTG and DDG an additional band of approximately 35 kDa was observed (Fig. 2a). The faster migrating band could represent a SDS-resistant conformation of β3AR-cc3.1 because many membrane proteins migrate faster on SDS-PAGE than their predicted molecular mass[43].

Therefore, analytical size exclusion chromatography was used in a next step to assess the monodispersity of the purified protein samples. As can be seen in Fig. 2b, a combination of DDM and cholesterol hemisuccinate (CHS) followed by FC12 and HEGA11 were the best detergents in terms of β3AR-cc3.1 monodispersity. Our findings are consistent with the observation that DDM/CHS was previously very successfully used for the purification of several GPCRs[44]. In the following we focused on the three best detergents identified in our experiments.

The thermostable SRS coiled coil significantly stabilizes β3AR.

Next, we assessed the thermal stability of β3AR-cc3.1 using the thiol-specific probe, 7-diethylamino-3-(4-maleimidophenyl)-4-methylcoumarin (CPM)[45]. The assay measures the fluorescence emission of CPM upon forming a covalent bond with the side chain of a free Cys. The free cysteine becomes more readily accessible upon protein thermal denaturation. β3AR-cc3.1 contains 14 cysteine residues. The CPM measurements were carried out in the range of 25–90 °C using a ramping rate of 2 °C/min to warrant equilibrium during unfolding without compromising the integrity
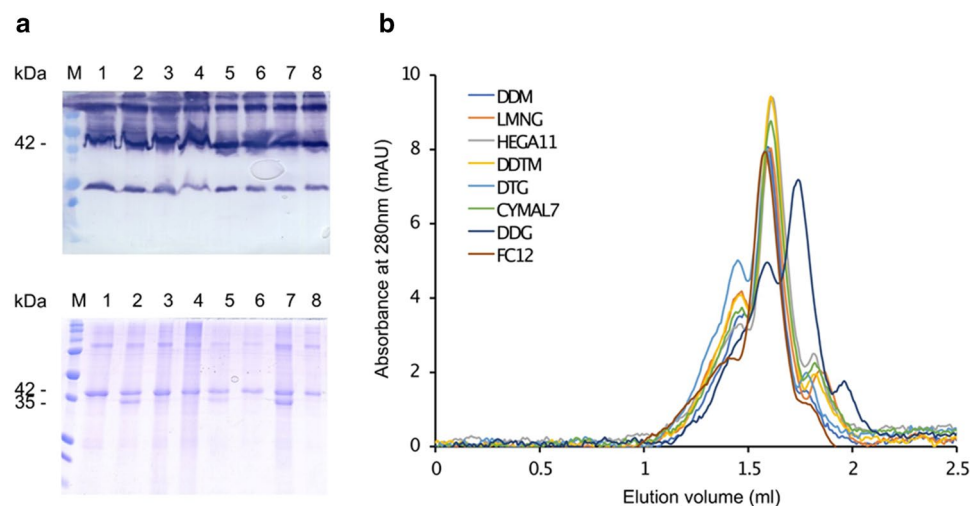

Figure 2. Solubilization, purification and monodispersity of β3AR-cc3.1. (**a**) Western blot (upper panel) and SDS-PAGE (lower panel) analysis of solubilization and purification of β3AR-cc3.1. All used detergents efficiently solubilized β3AR-cc3.1. The faster migrating band observed for some detergents could represent a SDS-resistant conformation of β3AR-cc3.1. Lane 1, DDM; lane 2, LMNG; lane 3, HEGA11; lane 4, DDTM; lane 5, DTG; lane 6, CYMAL7; lane 7, DDG, lane 8, FC12. The migration of marker proteins (M) is shown. (**b**) Analytical size exclusion chromatography for β3AR-cc3.1 purified in different detergents. The protein is eluting at a volume that corresponds to a monomer. Concerning monodispersity, the best detergent for the purification was DDM/CHS followed by FC12 and HEGA11.

of CPM. The thermal stability of β3AR-cc3.1 was tested with different ligands (antagonists: SR59230A, L748337 and carvedilol; agonist: carazolol), in Tris–HCl and HEPES buffers, and at different protein concentrations. For β3AR-cc3.1, a melting temperature (T_m) value of 65 °C was obtained in DDM/CHS and carvedilol (Fig. 3). In comparison, the T_m of thermostabilized β1AR was 55 °C[18], demonstrating that our approach is well suited to stabilize GPCRs. As expected, the stability of β3AR-cc3.1 was dependent on the type of detergent that was used. The T_m of the purified β3AR-cc3.1 decreased by 8 °C and 10 °C in the presence of HEGA11 and FC12, respectively (Fig. 3).

β3AR-cc3.1 maintains ligand-binding activity.   TM helices 5 and 6 play important roles for ligand binding and receptor activation[3]. Because our design approach to link TM helices 5 and 6 by a thermostable antiparallel coiled coil is expected to limit their conformational flexibility, it was important to assess the ligand binding properties of β3AR-cc3.1. To this end, saturation-binding assays were carried out with isolated HEK-239S-GnTI⁻ membranes expressing β3AR-cc3.1.

For these experiments, the antagonist [³H]-dihydroalprenolol (DHA) was used. Although DHA binding to β3AR-cc3.1 was not fully saturated at 300 nM, a K_D value of 150 nM was calculated (Fig. 4). A similar K_D value of ~ 100 nM was reported for the binding of alprenolol to β3AR[46], indicating that the engineered GPCR is still capable of binding to the antagonist ligand.

Although the ICL3 of most GPCRs is unstructured, our results are consistent with the observation that extended ICL3 structures are found in some natural GPCRs. For example, the ICL3 of squid rhodopsin[47] and bovine rhodopsin determined from its trigonal crystal[48] both form an extended anti-parallel helical structure
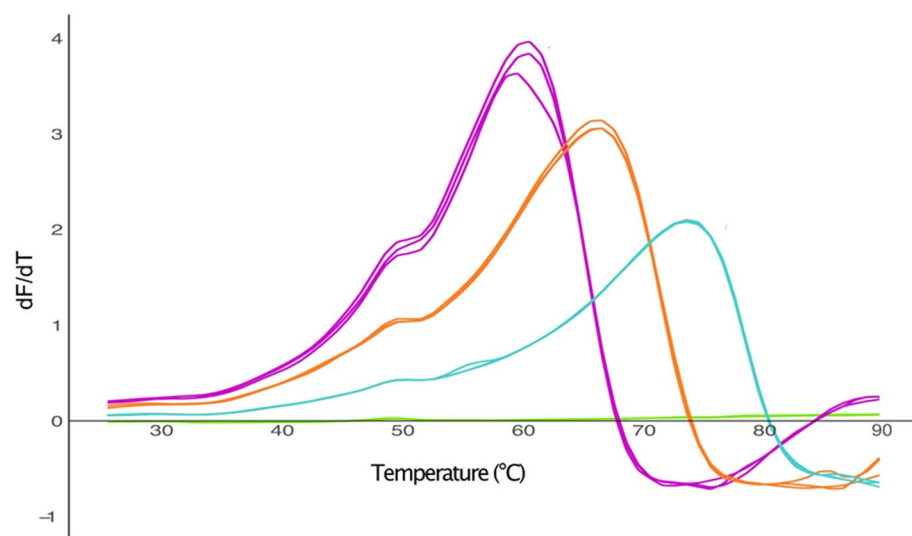
Figure 3. Thermal stability of β3AR-cc3.1. Replicate CPM measurements of β3AR-cc3.1 (15 µg) bound to carvedilol in different detergents. The apparent melting temperature of β3AR-cc3.1 in FC12 (purple) was 55 °C, 57 °C in HEGA11 (orange) and 65 °C in DDM/CHS (cyan). The light green curves represent measurements of the buffer without any protein.
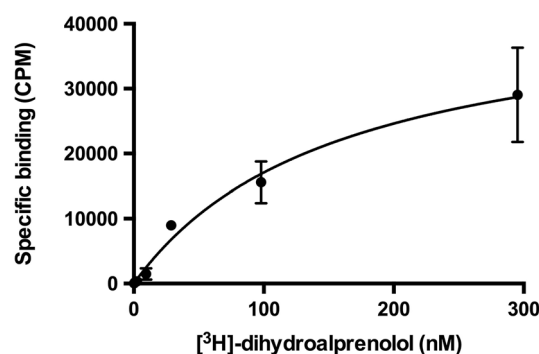
Figure 4. Saturation binding of antagonist [³H]-dihydroalprenolol to membranes from HEK-293S-GnTi⁻ cells expressing β3AR-cc3.1. Specific binding of [³H]-dihydroalprenolol obtained in saturation binding experiments with HEK-293S-GnTI⁻ membrane preparations expressing β3AR-cc3.1 is shown. A K_D value of 150 nM was calculated.

that is similar to an antiparallel coiled coil[25]. Although these findings indicate that our engineered GPCR chimera might possibly even still bind G proteins, stabilization of the helix 5–6 interface should directly affect signaling and therefore our chimeras might not be suitable to study GPCR signaling.

The coiled-coil fusion approach is well-suited for the stabilization of other GPCRs.
The general validity of our approach was tested by assessing other GPCRs. In the following, we will focus on the two receptors, the 5-hydroxytryptamine receptor 2C (5HTR2C) and the α-2B adrenergic receptor (α2BAR), that were purified, although successful expression tests have been done for several other GPCRs. Construct design was carried out as described for β3AR-cc3.1. 5HTR2C-cc contains two mutations (Asn204 and Asn205 to Qln), to avoid potential N-glycosylation that could prevent crystallization. No mutations were introduced into α2BAR-cc.

After the generation of stable cell lines, both proteins were expressed and purified as described for β3AR-cc3.1 using StrepTag Sepharose affinity chromatography and DDM/CHS as a detergent. 5HTR2C-cc and α2BAR-cc were purified in the presence of the antagonists mianserine and yohimbine, respectively. SDS-PAGE analysis revealed single bands migrating near the 37-kDa marker (Fig. 5). Although these results were very promising for the further characterization of the two chimeric receptors, we focused on β3AR-cc3.1.

β3AR-cc3.1 forms diffracting protein crystals.
Because biophysical characterization of β3AR-cc3.1 demonstrated that our coiled-coil-based approach is well suited for quickly and efficiently stabilizing the GPCR, we next aimed at crystallizing the engineered thermostabilized variant bound to carvedilol. Initially, vapor diffusion at 22 °C was employed using a protein concentration of 7.5 mg/mL. Extensive crystallization trials resulted in the formation of 30–70 μm-long needle-like crystals (Fig. 6a) of β3AR-cc3.1 in 0.2 M MgCl₂, 0.1 M sodium cacodylate pH 6.5 and 50% v/v PEG 200. Typically, the crystals grew within two hours and reached their maximal size after 3–4 days. Crystals displayed diffraction to approximately 22 Å (Fig. 6b). Intensive optimization was performed subsequently using different protein concentrations, additives, pHs, salts, buffers and precipitants, but there was no improvement in diffraction quality. We also tried to crystallize β3AR-cc3.1 using the lipidic cubic phase method, but did not obtain any crystals.

Increasing crystal contacts by replacing the loop connecting the α-helices of the SRS coiled coil by T4L.
Because we were not successful in optimizing conditions to obtain crystals that were suitable for structure determination, we decided to modify β3AR-cc3.1 on the protein level to improve crystal contacts. Truncation or mutation of the antiparallel coiled coil was not considered a valid option because the β3AR-cc3.1_SS and β3AR-cc3.2_SS variants failed to express, which was probably due to destabilization of the proteins. Although it has been reported that the loop connecting the two helices of an antiparallel coiled coil is crucial for the stability of the structure, it was demonstrated that substitution of the loop by a disulfide bond flanking the heptad repeats restored coiled-coil formation[35]. Although substitution of the connecting loop might alter the thermal stability of the antiparallel coiled coil, we decided to replace it with phage T4L. We selected T4L because it has been very successfully used as a fusion protein to crystallize and determine the structures of several GPCRs[11,19,20]. Because it crystallizes easily under many different conditions, T4L is considered an ideal fusion partner to establish crystal contacts. Another criterium for of choice was the existence of a β2AR crystal structure in which ICL3 was replaced by T4L. For the design, we used the structure-guided strategy described for the construction of β3AR-cc3.1. More specifically, we grafted the experimentally determined boundary of T4L to the coiled-coil like structure seen in β2AR on the antiparallel coiled coil of β3AR-cc3.1 (Fig. 7a,b).
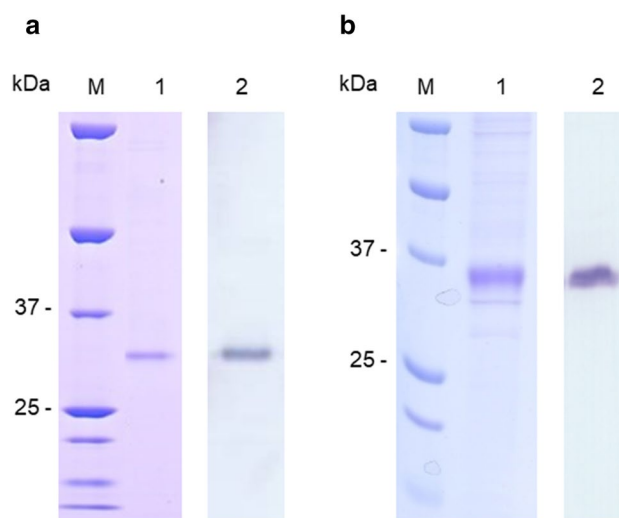
Figure 5. Purification of additional GPCRs demonstrate the feasibility of the coiled-coil fusion approach. SDS-PAGE (lane 1) and western blot (lane 2) analysis of purified 5HTR2C-cc (**a**) and α2BAR-cc (**b**). The migration of marker proteins (M) is shown.
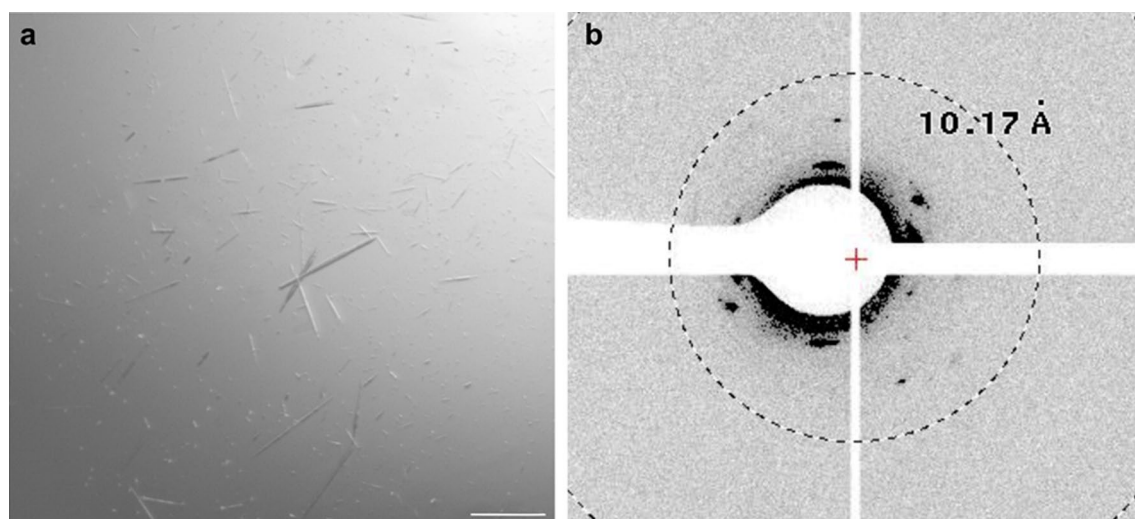
Figure 6. Crystallization of β3AR-cc3.1. (**a**) β3AR-cc3.1 crystals. The needles grew at a protein concentration of 7.5 mg in 0.2 M MgCl₂, 0.1 M sodium cacodylate pH 6.5 pH and 50% v/v PEG 200 in 3–4 days. Size bar, 10 μM. (**b**) X-ray diffraction pattern of β3AR-cc3.1 crystals. The crystals diffracted to a resolution of about 22 Å.
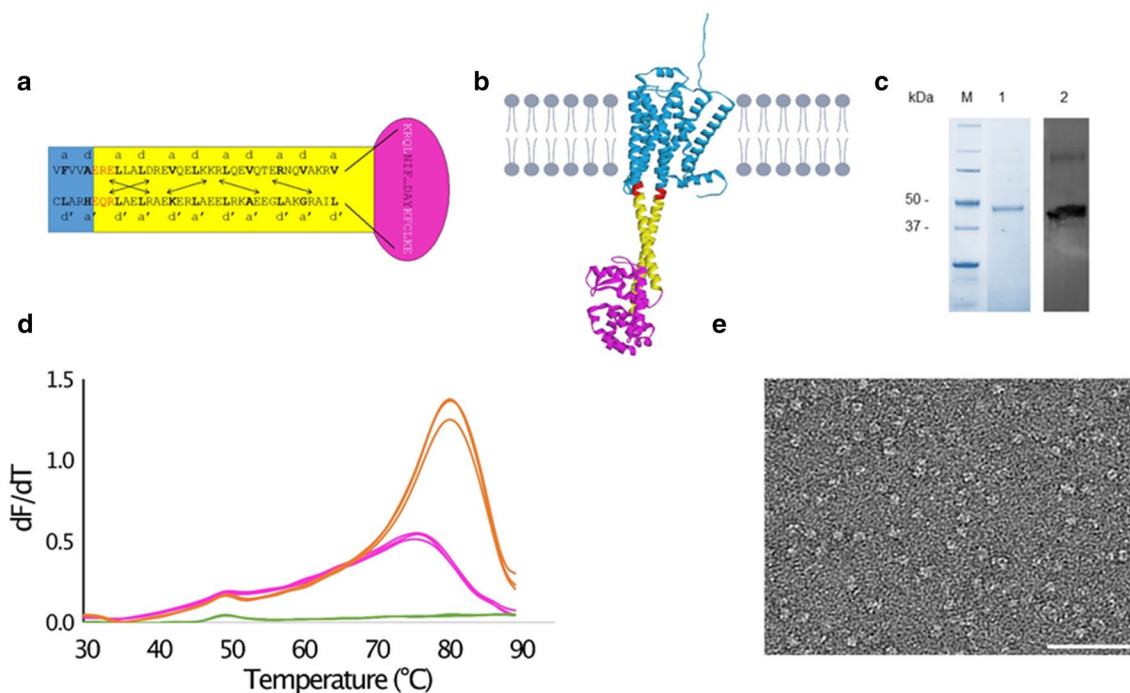
Figure 7. Design and characterization of β3AR-cc-T4L. (**a**) Design of β3AR-cc-T4L. For detail concerning the β3AR-cc3.1 part, see Fig. 1b. The T4L part is shown in magenta. The T4L sequence is in black and the connecting residues originating from β2AR are in white. (**b**) β3AR-cc-T4L model. β3AR is shown in blue, the cc3.1 coiled coil in yellow, T4L in magenta and residues at the junction in red. The model was generated by AlphaFold2[7]. (**c**) SDS-PAGE (lane 1) and western blot (lane 2) analysis of purified β3AR-cc-T4L. The migration of marker proteins (M) is shown. (**d**) Replicate CPM measurements of β3AR-cc3.1 (5 μg) and β3AR-cc-T4L (5 μg) bound to carvedilol in DDM. The T_m values of β3AR-cc3.1 (magenta) and β3AR-cc-T4L (orange) are 65 °C and 75 °C, respectively. The green curves represent measurements of the buffer without any protein. (**e**) Transmission electron micrograph of a negatively-stained β3AR-cc-T4L specimen. Scale bar, 50 nm.

Expression of the resulting variant, termed β3AR-cc-T4L, was only observed in T-REx-CHO cells (Fig. 7c). Despite we were not able to adapt stable cells for growth in suspension, we managed to purify a small amount of β3AR-cc-T4L for characterization from adherent T-REx-CHO cells using the best condition described for β3AR-cc3.1 (detergent combination DDM/CHS and antagonist carvedilol). Notably, β3AR-cc-T4L was significantly more stable than β3AR-cc3.1 and yielded a 10 °C higher T_m value of 75 °C (Fig. 7d). Therefore, β3AR-cc-T4L represents a promising candidate for crystallization.

Although the structure of the β3AR in its active state has recently been reported[49], β3AR-cc-T4L is also a potential candidate for structure determination of the inactive receptor by cryo-EM. It has a similar molecular weight as organic cation transporter-3 (62 kDa) for which a resolution of 3.2 Å has been obtained in recent studies[50]. Furthermore, to aid crystallization, β3AR-cc-T4L was designed to contain no flexible regions, which should also benefit cryo-EM studies. Therefore, we next tested the suitability of the engineered GPCR for cryo-EM analysis. Inspection of β3AR-cc-T4L molecules by transmission electron microscopy (TEM) after negative staining yielded a homogeneous distribution of uniformly appearing compact particles (Fig. 7e). This finding demonstrates that structure determination β3AR-cc-T4L by cryo-EM might be a promising approach, in particular in combination with a universal DARPin or nanobody that binds to T4L.

Conclusions

Structure determination of inactive-state GPCRs still mostly relies on X-ray crystallography. Based on the available GPCR crystal structures, a combination of protein stabilization and accessible soluble surface to establish crystal contacts would represent an ideal tool for crystallization. Towards this aim, we identified thermostable antiparallel coiled coils a such a tool. Preplacement of ICL3 of β3AR by cc3.1 resulted in significant stabilization of the GPCR while retaining its ligand-binding properties. Furthermore, we were also able to stabilize two other GPCRs, 5HTR2C and α2BAR (Fig. 5), demonstrating that this approach is generally suitable for the stabilization of GPCRs. Stabilization provides an attractive means for GPCRs that have only limited stability or are difficult to express. Furthermore, stabilized GPCRs appear also be of considerable interest for drug discovery applications because many drugs target the inactive state of the receptors.

Although we managed to crystallize the β3AR/coiled-coil chimera, the quality of the crystals even after extensive optimization was not suitable for structure determination. To supply additional surface for promoting crystal contacts, we replaced in a structure-based approach the loop connecting the helices of the antiparallel coiled coil by T4L. Although expression levels are currently not suitable for crystallization, we were able to show that the engineered GPCR is even more stable than the β3AR/coiled-coil chimera. TEM experiments demonstrated that GPCR-ccT4L fusions also represent promising candidate molecules for structure elucidation by cryo-EM.

The generation of the engineered GPCRs that led to a crystal structure often required many constructs for the optimal insertion of fusion proteins. It is therefore noteworthy that our structure-based approach is simple and straightforward. For all the examples described in this study, only the design of one construct was necessary to produce each protein.

Materials and methods

Constructs. Synthetic genes encoding the human β3 adrenergic receptor (β3AR, amino-acid residues Ala2 to Leu368 lacking Pro3 to Thr27) with the antiparallel coiled-coil sequences described in this study (Supplementary Table S1) inserted between Ala231 and Glu286 were codon-optimized for expression in human cells (Genewiz). Synthetic genes codon optimized for human cell expression and spanning amino-acid residues His3 to Trp450 of the human α-2B adrenergic receptor (α2BAR) and amino-acid residues Gly43 to Pro395 of the rat 5-hydroxytryptamine receptor 2C (5HTR2C) with cc3.1 inserted between Ala199 and Glu366 and Leu242 and Glu308, respectively, were purchased from Genewiz. The β3AR sequences also include the potentially thermo-stabilizing mutations Glu36Ala, Met86Val, Ile125Val, Glu126Trp, Tyr234Ala, Phe341Met, and Tyr346Leu[18,39]. In 5HTR2C two potential N-glycosylation sites (Asn204 and Asn205) were mutated to Gln. Insert sequences were further modified to contain a hemagglutinin signal sequence followed by a modified FLAG tag at the N-terminus and a TwinStrep tag that can be removed by thrombin or HRV 3C cleavage at the C-terminus (Supplementary Fig. S1). The full-length wild-type human β3AR cDNA sequence was used as a control. Insert sequences were subcloned into mammalian expression vectors pACMV-tetO[51] and pcDNA4/TO (ThermoFisher Scientific).

Cell culture and protein expression. Human embryonic kidney HEK293T (a gift from Prof. F.M. Wurm, EPFL, Switzerland to Prof. K. Ballmer-Hofer, Paul Scherrer Institute, Switzerland) were used for transient small-scale expression tests. HEK293T, T-REx-293, T-REx-CHO (from Thermo Fisher) and HEK293S GnTI[−51] were used for stable expression. Cells were transiently or stably transfected using 25 kDa branched PEI as described[52]. The cells were grown adherently and maintained at 37 °C in 5% CO$_2$ in Dulbecco's Modified Eagle Medium (DMEM) containing 10% fetal calf serum (FCS), penicillin (100 U/mL), streptomycin (100 µg/mL) and L-glutamine (2 mM).

Stable cell lines were generated by using geneticin (G-418, 0.2 mg/mL) or zeocin (0.4 mg/mL) for pACMV-tetO and pcDNA4/TO, respectively. Individual colonies (24 for each receptor construct) typically appeared after 14 days and were isolated and expanded as described before[51]. Protein expression was induced with tetracycline (2 µg/mL) and sodium butyrate (5 mM) and cells further incubated for 72 h. For each clone, the expression level of the recombinant protein was assessed by western blotting, and the best clones were selected for further large-scale expression in suspension. Stably transfected cells were grown in suspension in a final volume of 5 × 1 L of PEM media (5% fetal calf serum (FCS), 1% (pyrrolidone carboxylic acid) PSA, 2.5 mM Glutamax). Expression was induced upon reaching a cell density of ~ 3 × 10^6 cells/mL as described above. Cells were harvested after 72 h by centrifugation at 2500g, frozen in liquid nitrogen and stored at − 80 °C for protein purification or washed twice with PBS prior to freezing for membrane preparations.

Membrane preparation and protein purification. For membrane preparation, cells were thawed on ice for 30 min. The cells were lysed in 20 mM Tris, pH 8, 500 mM NaCl, 15% glycerol, 50 mg/L DNAse I, 1 tablet/5 L cell suspension of the EDTA-Free cOmplete Protease Inhibitor Cocktail (Roche) and 20 µM carvedilol using a continuous flow EmulsiFlex-C3 cell disruptor (Avestin). The cell lysate was centrifuged at 10,000g for

30 min at 4 °C, followed by centrifugation of the resulting supernatant at 100,000*g* for 1 h at 4 °C. The membranes were flash-frozen in liquid nitrogen and stored at − 80 °C for further use.

For protein purification, membranes were thawed on ice and solubilized using 1% (w/v) *n*-dodecyl-β-ᴅ-maltopyranoside (DDM, Anatrace), 0.2% (w/v) cholesteryl hemisuccinate (CHS, Sigma-Aldrich) in 50 mM Tris pH 7.5, 150 mM NaCl containing 20 μM carvedilol (β3AR), 20 μM mianserine (5HTR2C) or 500 nM yohimbine (α2BAR) (TOCRIS) for 45 min at 4 °C on roller shaker. The insoluble material was separated by high-speed centrifugation at 100,000*g* for 1 h at 4 °C. The supernatant was loaded on a StrepTrap Sepharose High-Performance column (MERCK) equilibrated with 50 mM Tris pH 7.8 and 150 mM NaCl supplemented with 0.05% DDM, 0.01% CHS and 20 μM carvedilol (β3AR), 20 μM mianserine (5HTR2C) or 500 nM yohimbine (α2BAR). The proteins were washed with 10 column volumes of 50 mM Tris pH 7.8, 150 mM NaCl, 0.05% DDM, 0.01% CHS, 20 μM carvedilol (β3AR) or 500 nM yohimbine (α2BAR) and eluted with 4 column volumes of 50 mM Tris pH 7.8, 150 mM NaCl, 0.05% DDM, 0.01% CHS, 20 μM carvedilol (β3AR), 20 μM mianserine (5HTR2C) or 500 nM yohimbine (α2BAR) and 2.5 mM desthiobiotin. For size-exclusion chromatography (SEC) of β3AR variants, a HiLoad 10/30 Superdex-200 column (Cytiva) was used. The buffer used for SEC was 50 mM Tris pH 7.8, 150 mM NaCl, 0.05% DDM and 0.02% CHS and 20 μM carvedilol. The protein samples were concentrated to 30 mg/mL using 100-kDa MWCO AmiconUltra concentrators (Millipore) for crystallization trials and further analysis.

β3ARcc3.1 crystallization.
β3ARcc3.1 bound to carvedilol was concentrated to 10 mg/mL and crystallized by sitting-drop vapor diffusion at 20 °C using a TPP Mosquito robot. Proteins were mixed with the reservoir solution using a volume ratio of 1:1 (200 nl each). Crystals of β3AR-cc3.1 were obtained in 0.2 M MgCl$_2$, 0.1 M sodium cacodylate pH 6.5 and 50% v/v PEG 200. Crystals typically appeared within 4 h and grew to their maximum size of 14 × 5 × 3 μm within 2 days. Diffraction experiments performed at beamline PXI (Swiss Light Source, Villigen, Switzerland) equipped with an EIGER 16M high resolution diffractometer (Dectris) confirmed the existence of protein crystals. Subsequently, manual optimization of β3ARcc3.1 crystals was tried at a protein concentration of 15 mg/mL.

Radioligand binding assay.
Membrane preparations ranged between 0.25–2 μg of protein/well. The radioligand binding experiments were done in a volume of 200 μl (50 μl Hanks' Balanced Salt Solution (HBSS) assay buffer, 20 mM HEPES, 0.1% BSA, pH 7.4; 25 μl antagonist or assay buffer (depending on assay type), 50 μl membrane solution (final protein concentration 5 μg), 50 μl scintillation proximity assay (SPA) solution (Perkin Elmer), and 25 μl of dihydroalprenolol hydrochloride, levo-[ring, propyl-^{3}H(N)] (PerkinElmer). For saturation binding experiments, we used up to 300 nM of [3H]-dihydroalprenolol. Different dilutions of the radioligand were prepared in assay buffer corresponding to a concentration range of approximately 0.02–300 nM. Non-specific binding was determined in the presence of 10 μM of the selective β3 antagonist L748337 (TOCRIS). Samples were incubated in 96-well plate sealed with transparent Topseal for 2 h at 25 °C with gentle agitation. Samples were centrifuged for 10 min at 2500*g* before being analyzed in a β-counter. Data were fitted using a nonlinear regression, one site binding model with GraphPad Prism 6.0 (GraphPad Software, Inc.).

Thermostability assay.
Thermal stability of proteins was assessed the fluorescent cysteine-reactive dye, 7-diethylamino-3-(4-maleimidophenyl)-4-methylcoumarin (CPM) as described before[45]. The protein concentration used per assay was 5–10 μg. Thermal unfolding was monitoring using the Qiagen Rotor-Gene Q instrument. Excitation was at 365 nm and emission at 460 nm was recorded over a temperature range from 25 to 90 °C with a ramping rate of 2 °C/min. Data analysis was performed using the Rotor-Gene software.

Transmission electron microscopy (TEM).
Negative stain images of B3ARccT4L were made by applying one drop of protein sample (10 μg/mL) onto a glow-discharged carbon coated copper EM grid for 60 s. The grid was washed with three drops of distilled water, one drop of 2% uranyl acetate and subsequently placed on a drop of 2% uranyl acetate for 10 s, blotted with a filter paper and allowed to air dry. Negatively stained EM grids were observed on a Talos L120C microscope (Thermo Fisher Scientific, USA), operated at 120 kV. Images were recorded at a nominal magnification of 120,000 × using a Ceta CMOS camera, corresponding to a pixel size of 1.2 Å/pixel on the specimen. TEM images were analyzed by the image analysis tool ImageJ (NIH).

Data availability
All the data used in this paper are available from the corresponding author on reasonable request.

References

1. Katritch, V., Cherezov, V. & Stevens, R. C. Structure–function of the G protein-coupled receptor superfamily. *Annu. Rev. Pharmacol. Toxicol.* **53**, 531–556. https://doi.org/10.1146/annurev-pharmtox-032112-135923 (2013).
2. Hilger, D., Masureel, M. & Kobilka, B. K. Structure and dynamics of GPCR signaling complexes. *Nat. Struct. Mol. Biol.* **25**, 4–12. https://doi.org/10.1038/s41594-017-0011-7 (2018).
3. Weis, W. I. & Kobilka, B. K. The molecular basis of G protein-coupled receptor activation. *Annu. Rev. Biochem.* **87**, 897–919. https://doi.org/10.1146/annurev-biochem-060614-033910 (2018).
4. Congreve, M., de Graaf, C., Swain, N. A. & Tate, C. G. Impact of GPCR structures on drug discovery. *Cell* **181**, 81–91. https://doi.org/10.1016/j.cell.2020.03.003 (2020).

5. Hauser, A. S., Attwood, M. M., Rask-Andersen, M., Schioth, H. B. & Gloriam, D. E. Trends in GPCR drug discovery: New agents, targets and indications. *Nat. Rev. Drug Discov.* **16**, 829–842. https://doi.org/10.1038/nrd.2017.178 (2017).
6. Santos, R. *et al.* A comprehensive map of molecular drug targets. *Nat. Rev. Drug Discov.* **16**, 19–34. https://doi.org/10.1038/nrd.2016.230 (2017).
7. Jumper, J. *et al.* Highly accurate protein structure prediction with AlphaFold. *Nature* **596**, 583–589. https://doi.org/10.1038/s41586-021-03819-2 (2021).
8. Baek, M. *et al.* Accurate prediction of protein structures and interactions using a three-track neural network. *Science* **373**, 871–876. https://doi.org/10.1126/science.abj8754 (2021).
9. Garcia-Nafria, J. & Tate, C. G. Structure determination of GPCRs: Cryo-EM compared with X-ray crystallography. *Biochem. Soc. Trans.* **49**, 2345–2355. https://doi.org/10.1042/BST20210431 (2021).
10. Robertson, M. J. *et al.* Structure determination of inactive-state GPCRs with a universal nanobody. *Nat. Struct. Mol. Biol.* **29**, 1188–1195. https://doi.org/10.1038/s41594-022-00859-8 (2022).
11. Chun, E. *et al.* Fusion partner toolchest for the stabilization and crystallization of G protein-coupled receptors. *Structure* **20**, 967–976. https://doi.org/10.1016/j.str.2012.04.010 (2012).
12. Jaeger, K. *et al.* Structural basis for allosteric ligand recognition in the human CC chemokine receptor 7. *Cell* **178**, 1222-1230 e1210. https://doi.org/10.1016/j.cell.2019.07.028 (2019).
13. Yin, J., Mobarec, J. C., Kolb, P. & Rosenbaum, D. M. Crystal structure of the human OX2 orexin receptor bound to the insomnia drug suvorexant. *Nature* **519**, 247–250. https://doi.org/10.1038/nature14035 (2015).
14. Popov, P., Kozlovskii, I. & Katritch, V. Computational design for thermostabilization of GPCRs. *Curr. Opin. Struct. Biol.* **55**, 25–33. https://doi.org/10.1016/j.sbi.2019.02.010 (2019).
15. Kang, Y. *et al.* Crystal structure of rhodopsin bound to arrestin by femtosecond X-ray laser. *Nature* **523**, 561–567. https://doi.org/10.1038/nature14656 (2015).
16. Deluigi, M. *et al.* Complexes of the neurotensin receptor 1 with small-molecule ligands reveal structural determinants of full, partial, and inverse agonism. *Sci. Adv.* **7**, abe5504. https://doi.org/10.1126/sciadv.abe5504 (2021).
17. Rasmussen, S. G. *et al.* Crystal structure of the human beta2 adrenergic G-protein-coupled receptor. *Nature* **450**, 383–387. https://doi.org/10.1038/nature06325 (2007).
18. Serrano-Vega, M. J., Magnani, F., Shibata, Y. & Tate, C. G. Conformational thermostabilization of the beta1-adrenergic receptor in a detergent-resistant form. *Proc. Natl. Acad. Sci. U.S.A.* **105**, 877–882. https://doi.org/10.1073/pnas.0711253105 (2008).
19. Cherezov, V. *et al.* High-resolution crystal structure of an engineered human beta2 adrenergic G protein-coupled receptor. *Science* **318**, 1258–1265. https://doi.org/10.1126/science.1150577 (2007).
20. Rosenbaum, D. M. *et al.* GPCR engineering yields high-resolution structural insights into beta2-adrenergic receptor function. *Science* **318**, 1266–1273. https://doi.org/10.1126/science.1150609 (2007).
21. Warne, T. *et al.* Structure of a beta1-adrenergic G-protein-coupled receptor. *Nature* **454**, 486–491. https://doi.org/10.1038/nature07101 (2008).
22. Oswald, C. *et al.* Intracellular allosteric antagonism of the CCR9 receptor. *Nature* **540**, 462–465. https://doi.org/10.1038/nature20606 (2016).
23. Dore, A. S. *et al.* Structure of class C GPCR metabotropic glutamate receptor 5 transmembrane domain. *Nature* **511**, 557–562. https://doi.org/10.1038/nature13396 (2014).
24. Wu, B. *et al.* Structures of the CXCR4 chemokine GPCR with small-molecule and cyclic peptide antagonists. *Science* **330**, 1066–1071. https://doi.org/10.1126/science.1194396 (2010).
25. Lupas, A. Prediction and analysis of coiled-coil structures. *Methods Enzymol.* **266**, 513–525. https://doi.org/10.1016/s0076-6879(96)66032-7 (1996).
26. Weissenhorn, W., Dessen, A., Harrison, S. C., Skehel, J. J. & Wiley, D. C. Atomic structure of the ectodomain from HIV-1 gp41. *Nature* **387**, 426–430. https://doi.org/10.1038/387426a0 (1997).
27. Kammerer, R. A. *et al.* Interaction of agrin with laminin requires a coiled-coil conformation of the agrin-binding site within the laminin gamma1 chain. *EMBO J.* **18**, 6762–6770. https://doi.org/10.1093/emboj/18.23.6762 (1999).
28. Cho, C. H. *et al.* COMP-Ang1: A designed angiopoietin-1 variant with nonleaky angiogenic activity. *Proc. Natl. Acad. Sci. U.S.A.* **101**, 5547–5552. https://doi.org/10.1073/pnas.0307574101 (2004).
29. Deiss, S. *et al.* Your personalized protein structure: Andrei N. Lupas fused to GCN4 adaptors. *J. Struct. Biol.* **186**, 380–385. https://doi.org/10.1016/j.jsb.2014.01.013 (2014).
30. O'Shea, E. K., Klemm, J. D., Kim, P. S. & Alber, T. X-ray structure of the GCN4 leucine zipper, a two-stranded, parallel coiled coil. *Science* **254**, 539–544. https://doi.org/10.1126/science.1948029 (1991).
31. Testa, O. D., Moutevelis, E. & Woolfson, D. N. CC+: A relational database of coiled-coil structures. *Nucleic Acids Res.* **37**, D315–D322. https://doi.org/10.1093/nar/gkn675 (2009).
32. Gupta, K., Sharp, R., Yuan, J. B., Li, H. & Van Duyne, G. D. Coiled-coil interactions mediate serine integrase directionality. *Nucleic Acids Res.* **45**, 7339–7353. https://doi.org/10.1093/nar/gkx474 (2017).
33. Boudko, S. P., Kuhn, R. J. & Rossmann, M. G. The coiled-coil domain structure of the Sin Nombre virus nucleocapsid protein. *J. Mol. Biol.* **366**, 1538–1544. https://doi.org/10.1016/j.jmb.2006.12.046 (2007).
34. Fujinaga, M., Berthet-Colominas, C., Yaremchuk, A. D., Tukalo, M. A. & Cusack, S. Refined crystal structure of the seryl-tRNA synthetase from *Thermus thermophilus* at 2.5 A resolution. *J. Mol. Biol.* **234**, 222–233. https://doi.org/10.1006/jmbi.1993.1576 (1993).
35. Oakley, M. G. & Kim, P. S. Protein dissection of the antiparallel coiled coil from *Escherichia coli* seryl tRNA synthetase. *Biochemistry* **36**, 2544–2549. https://doi.org/10.1021/bi962391t (1997).
36. Brauning, B. *et al.* Structure and mechanism of the two-component alpha-helical pore-forming toxin YaxAB. *Nat. Commun.* **9**, 1806. https://doi.org/10.1038/s41467-018-04139-2 (2018).
37. Carter, A. P. *et al.* Structure and functional role of dynein's microtubule-binding domain. *Science* **322**, 1691–1695. https://doi.org/10.1126/science.1164424 (2008).
38. Kraatz, S. H. W., Bianchi, S. & Steinmetz, M. O. Combinatorial use of disulfide bridges and native sulfur-SAD phasing for rapid structure determination of coiled-coils. *Biosci. Rep.* https://doi.org/10.1126/science.1164424 (2018).
39. Miller-Gallacher, J. L. *et al.* The 2.1 A resolution structure of cyanopindolol-bound beta1-adrenoceptor identifies an intramembrane Na+ ion that stabilises the ligand-free receptor. *PLoS One* **9**, e92727. https://doi.org/10.1371/journal.pone.0092727 (2014).
40. Serrano-Vega, M. J. & Tate, C. G. Transferability of thermostabilizing mutations between beta-adrenergic receptors. *Mol. Membr. Biol.* **26**, 385–396. https://doi.org/10.3109/09687680903208239 (2009).
41. Tripet, B., Wagschal, K., Lavigne, P., Mant, C. T. & Hodges, R. S. Effects of side-chain characteristics on stability and oligomerization state of a de novo-designed model coiled-coil: 20 amino acid substitutions in position "d". *J. Mol. Biol.* **300**, 377–402. https://doi.org/10.1006/jmbi.2000.3866 (2000).
42. Wagschal, K., Tripet, B., Lavigne, P., Mant, C. & Hodges, R. S. The role of position a in determining the stability and oligomerization state of alpha-helical coiled coils: 20 amino acid stability coefficients in the hydrophobic core of proteins. *Protein Sci.* **8**, 2312–2329. https://doi.org/10.1110/ps.8.11.2312 (1999).
43. Rath, A., Glibowicka, M., Nadeau, V. G., Chen, G. & Deber, C. M. Detergent binding explains anomalous SDS-PAGE migration of membrane proteins. *Proc. Natl. Acad. Sci. U.S.A.* **106**, 1760–1765. https://doi.org/10.1073/pnas.0813167106 (2009).

44. Kulig, W. *et al.* How well does cholesteryl hemisuccinate mimic cholesterol in saturated phospholipid bilayers?. *J. Mol. Model.* **20**, 2121. https://doi.org/10.1007/s00894-014-2121-z (2014).
45. Alexandrov, A. I., Mileni, M., Chien, E. Y., Hanson, M. A. & Stevens, R. C. Microscale fluorescent thermal stability assay for membrane proteins. *Structure* **16**, 351–359. https://doi.org/10.1016/j.str.2008.02.004 (2008).
46. Baker, J. G. The selectivity of beta-adrenoceptor antagonists at the human beta1, beta2 and beta3 adrenoceptors. *Br. J. Pharmacol.* **144**, 317–322. https://doi.org/10.1038/sj.bjp.0706048 (2005).
47. Murakami, M. & Kouyama, T. Crystal structure of squid rhodopsin. *Nature* **453**, 363–367. https://doi.org/10.1038/nature06925 (2008).
48. Palczewski, K. *et al.* Crystal structure of rhodopsin: A G protein-coupled receptor. *Science* **289**, 739–745. https://doi.org/10.1126/science.289.5480.739 (2000).
49. Nagiri, C. *et al.* Cryo-EM structure of the beta3-adrenergic receptor reveals the molecular basis of subtype selectivity. *Mol. Cell* **81**, 3205-3215 e3205. https://doi.org/10.1016/j.molcel.2021.06.024 (2021).
50. Khanppnavar, B. *et al.* Structural basis of organic cation transporter-3 inhibition. *Nat. Commun.* **13**, 6714. https://doi.org/10.1038/s41467-022-34284-8 (2022).
51. Reeves, P. J., Kim, J. M. & Khorana, H. G. Structure and function in rhodopsin: A tetracycline-inducible system in stable mammalian cell lines for high-level expression of opsin mutants. *Proc. Natl. Acad. Sci. U.S.A.* **99**, 13413–13418. https://doi.org/10.1073/pnas.212519199 (2002).
52. Chaudhary, S., Pak, J. E., Gruswitz, F., Sharma, V. & Stroud, R. M. Overexpressing human membrane proteins in stably transfected and clonal human embryonic kidney 293S cells. *Nat. Protoc.* **7**, 453–466. https://doi.org/10.1038/nprot.2011.453 (2012).

Author contributions

R.A.K. conceptualization; M.A. and R.A.K. data curation; M.A., O.L., P.J., D.F. and X.L. formal analysis, investigation and validation; R.A.K. and X.L. funding acquisition and supervision; M.A. and R.A.K. writing—review and editing and writing original draft with input from the other authors.

Competing interests

The authors declare no competing interests.

Additional information

Supplementary Information The online version contains supplementary material available at https://doi.org/10.1038/s41598-023-36855-1.

Correspondence and requests for materials should be addressed to R.A.K.

Reprints and permissions information is available at www.nature.com/reprints.

Publisher's note Springer Nature remains neutral with regard to jurisdictional claims in published maps and institutional affiliations.